Bio-Optics of the Chesapeake Bay from Measurements and Radiative Transfer Calculations

Maria Tzortziou [1]
Jay R. Herman [2]
Charles L. Gallegos [3]
Patrick J. Neale [3]
Ajit Subramaniam [4]
Lawrence W. Harding Jr, [5]
Ziauddin Ahmad [6]

[1] University of Maryland, Earth System Science Interdisciplinary Center
College Park, MD, 20742, USA

[2] NASA/Goddard Space Flight Center
Greenbelt, MD, 20771, USA

[3] Smithsonian Environmental Research Center
Edgewater, MD, 21037, USA

[4] Lamont Doherty Earth Observatory, Columbia University
Palisades, NY, 10964, USA

[5] University of Maryland, Horn Point Laboratory
Cambridge, MD 21613, USA

[6] Science and Data Systems, Inc.,
Silver Spring, MD, 20906, USA

Running header: Bio-optical characteristics and radiative transfer closure in Chesapeake Bay

Abstract

We combined detailed bio-optical measurements and radiative transfer (RT) modeling to perform an 'optical closure' experiment for optically complex and biologically productive Chesapeake Bay waters. We used this experiment to evaluate certain assumptions commonly used when modeling bio-optical processes, and to investigate the relative importance of several optical characteristics needed to accurately model and interpret remote sensing ocean-color observations in these Case 2 waters. Direct measurements were made of the magnitude, variability, and spectral characteristics of backscattering and absorption that are critical for accurate parameterizations in satellite bio-optical algorithms and underwater RT simulations. We found that the ratio of backscattering to total scattering (i.e. the backscattering fraction, b_b/b) in the mid-mesohaline Chesapeake Bay varied considerably depending on particulate loading, distance from land, and mixing processes, and had an average value of 0.0128 at 530 nm. Incorporating information on the magnitude, variability, and spectral characteristics of particulate backscattering into the RT model, rather than using a volume scattering function commonly assumed for turbid waters, was critical to obtaining agreement between RT calculations and measured radiometric quantities. In situ measurements of absorption coefficients need to be corrected for systematic overestimation due to scattering errors, and this correction commonly employs the assumption that absorption by particulate matter at near infrared wavelengths is zero. Direct measurements, however, showed that particulate matter in the Bay had small, but non-zero absorption in the 700-730 nm wavelength region. Accounting for this residual particulate absorption when correcting in-situ measured absorption spectra for scattering errors was important in RT model simulations of water reflectance in the green wavelengths, where reflectance spectra in estuarine waters peak. Sun-induced chlorophyll

fluorescence considerably affected the magnitude of water reflectance at the red wavelengths. Very good RT optical closure was obtained between independently measured water inherent optical properties and radiation fields, after applying the results from our detailed measurements to model bio-optical processes in these Case 2 waters. The good optical closure was consistent over the observed wide range of water optical characteristics. Average absolute percent differences between measured and model-estimated water-leaving radiances were on the order of 6.35% at 443 nm, 7.73% at 554 nm, and 6.86% at 670 nm, considerably smaller than those presented in the few studies of optical closure performed previously in near shore waters of similar optical complexity. These results show that bio-optical processes can be confidently modeled in complex estuarine waters, and underscore the importance of accurate formulations for backscattering, long wavelength particulate absorption, and chlorophyll fluorescence.

Keywords: optical closure; backscattering; chlorophyll fluorescence; particulate absorbance; remote sensing; estuaries; coastal waters

1. Introduction

Remote sensing of ocean color is based on measurements of light that leaves the water surface and reaches an aircraft or satellite-borne sensor, carrying with it information about the water optical characteristics. High concentrations of optically active, non-covarying, biogeochemical constituents, such as phytoplankton, colored dissolved organic matter (CDOM), and non-algal particles, influence ocean color in estuarine and coastal regions. In order to use remote sensing to estimate changes in coastal water composition and biological activity it is necessary to develop appropriate, and in many cases 'regionally-specific', bio-optical algorithms relating the remotely sensed water reflectance to the optical properties (i.e. absorption and scattering) of the individual, optically-active water constituents (e.g. Garver and Siegel, 1997; Carder et al., 1999; Maritorena et al., 2002). However, for many estuarine and coastal waters certain optical properties (e.g. particulate backscattering) remain poorly characterized (e.g. Babin et al., 2003; Magnuson et al., 2004). Therefore, specific, in-situ data on how these properties affect water reflectance in the visible are needed for effective interpretation of remotely sensed ocean color in near shore regions.

Development of effective coastal bio-optical algorithms and validation of remote sensing observations using in-situ bio-optical data requires testing the accuracy of the data and the consistency, or 'optical closure', among the independently measured quantities. Demonstration of optical closure involves solution of the equations of radiative transfer (RT) using measured boundary conditions (e.g. incident radiance) and inherent optical properties (IOPs) to predict independent measurements of apparent optical properties, such as downwelling irradiance (Ed(λ,z)), or remote sensing reflectance (Rrs(λ)). RT modeling can be used to investigate errors in measurement methodology and uncertainties in relationships used in bio-optical models, as

well as examine the relative importance of several bio-optical processes in determining coastal ocean color (schematic illustration shown in Figure 1). However, very few studies have been published on optical closure for optically complex near shore waters (e.g. Chang et al., 2003; Bulgarelli et al., 2003).

Three bio-optical properties, for which in-situ determinations remain scarce, are particularly important to effective interpretation of coastal ocean color: (i) variability in particulate backscattering, b_b, and the ratio of backscattering to total scattering by particles, i.e. backscattering fraction, b_b/b (e.g. Mobley et al., 2002); (ii) long wavelength non-algal particulate absorption characteristics (e.g. Babin and Stramski, 2002; Tassan and Ferrari, 2003); and (iii) contribution of solar-induced chlorophyll fluorescence to remotely-sensed water reflectance (e.g. Gower, 1980; Maritorena et al., 2000). The *R*rs, defined by the ratio of water leaving radiance, *L*w, to downwelling surface irradiance, *E*s, is to a first approximation proportional to the ratio of backscattering to absorption, b_b/a, (e.g. Morel and Prieur, 1977). Thus, both backscattering and absorption are important in determining the magnitude and spectral shape of water reflectance. However, information on particulate backscattering magnitude, spectral shape, or angular dependence is extremely scarce for estuarine and coastal waters. As a result, modeling of backscattering processes has been largely based on a few existing datasets and assumptions regarding b_b/b variability. For example, the Petzold 'average particle' volume scattering function (VSF) (Petzold, 1972), derived from three measurements of VSF in San Diego Harbor and with an estimated b_b/b of 0.018, has been widely assumed for modeling b_b in coastal waters. The lack of direct measurements of b_b poses a significant limitation in the development of appropriate backscattering parameterizations for coastal satellite algorithms, or the evaluation of remote sensing backscattering products (e.g. Magnuson et al., 2004). Water absorption properties are

more frequently measured as part of near shore water-quality studies. In-situ measurements of dissolved and particulate absorption characteristics have been made in estuarine and coastal waters by several ship-based monitoring programs during the last decades (e.g. Tassan 1988; Carder et al., 1989; Roesler et al., 1989; Magnuson et al., 2004). However, current understanding of variations in the non-algal particulate absorption spectra is still limited (Babin et al., 2003) and uncertainties remain about the long-wavelength particulate absorption in highly turbid waters. When using in situ measurements of total absorption for RT modeling in coastal waters, small errors at green wavelengths, where the absorption spectrum has a broad minimum, can amplify errors in estimation of *R*rs. Ramifications of assuming zero particulate absorption at near-infrared wavelengths when correcting in situ absorption measurements at green wavelengths for scattering bias (e.g. Zaneveld et al., 1994) have not been explored. Sun-induced chlorophyll fluorescence affects the magnitude and spectral shape of reflectance in natural waters (e.g. Gordon, 1979; Maritorena et al., 2000). The remotely sensed chlorophyll fluorescence signal can be strong in estuaries like the Chesapeake Bay that are characterized by high chlorophyll concentrations. Optical closure studies provide a means of evaluating the effect of chlorophyll fluorescence on *R*rs and, consequently, a basis for remote sensing retrieval of chlorophyll.

Chesapeake Bay is a large and biologically productive estuary characterized by Case 2 waters with strong backscattering and absorption by non-covarying dissolved and particulate components (e.g. Harding et al., 2005; Tzortziou, 2004). Remote sensing is a potentially powerful tool for studying phytoplankton dynamics and managing water quality in the Chesapeake Bay by virtue of its ability to resolve steep spatial gradients and temporal variability in optically active constituents (Harding et al., 2005). Strong riverine dependence of all optically

active constituents, however, means that each of the three factors listed above complicates successful retrieval of key properties from remote sensing (Magnuson et al., 2004). An approach combining new in situ measurements of particulate backscattering and absorption with RT modeling in Chesapeake Bay is needed to resolve the difficulties imposed by the optical complexities.

In this paper we present an analysis of in-situ, bio-optical measurements for the mid-mesohaline Chesapeake Bay, including direct measurements of the magnitude, variability and spectral characteristics of particulate backscattering and absorption. We then apply our measurements to RT model simulations of underwater radiation fields using the Hydrolight code (Mobley, 1988). Our main objective was to use a combination of detailed bio-optical data with RT closure results to evaluate: (i) alternative formulations for the backscattering processes in these waters, and the importance of accurate representation of backscattering in RT calculations; (ii) long-wavelength particulate absorption and its effect, as well as that of chlorophyll fluorescence, on RT model simulations of R_{rs} spectra; (iii) the consistency and optical closure among independently measured IOPs and radiometric quantities, as a step towards applying these data to the interpretation of satellite observations and the investigation of bio-optical relationships for improved remote sensing retrievals in these Case 2 waters.

2. Material and Methods

2.1. Location and duration of measurements

Measurements of inherent optical characteristics and water quality were made at four stations in the Chesapeake Bay designated: Poplar Island (PI), Herring Bay (HB), Tilghman Island (TI) and Jetta (JT) (38.71°-38.89° N latitude, 76.34°-76.54° W longitude) (Figure 2). This region included the turbid, lateral portions of the upper Bay, as well as a portion of the mid-channel. Measurements were made during 17 cruises performed between June 2001 and November 2002 (Table 1).

2.2. In-situ measurements and calculations

In-situ vertical profiles of total (minus pure water) attenuation, $c_{t\text{-}w}(\lambda, z)$, and absorption, $a_{t\text{-}w}(\lambda, z)$, were measured at nine visible wavelengths using a WETLabs Spectral AC-9. Temperature and salinity were measured with Hydrolab Datasonde 4a, and these data were used to correct AC9 measurements for the temperature and salinity dependence of absorption by pure water (Pegau et al., 1997). Total particulate scattering, $b_p(\lambda, z)$, was estimated as the difference between $c_{t\text{-}w}(\lambda, z)$ and $a_{t\text{-}w}(\lambda, z)$, after applying additional corrections to account for scattering losses manifested as overestimates of measured absorption (Kirk, 1992). We initially corrected the AC9 measurements for scattering errors according to Zaneveld et al. (1994). This correction is based on the assumption that the sum of particulate and dissolved absorption at 715 nm is zero. The correction is applied by subtracting a fraction of the AC9 measured scattering from the whole measured absorption spectrum. The fraction is scaled to set non-water absorption at 715 nm to zero. That is,

$$a_{t-w}(\lambda)_{corrected} = a_{t-w}(\lambda)_{measured} - \frac{a_{t-w}(715)_{measured}}{b_{t-w}(715)_{measured}} b_{t-w}(\lambda)_{measured} \quad (1)$$

Based on two lines of evidence in our results (see below, Results and Discussion), we modified this correction to allow for non-zero particulate absorption at 715 nm.

An ECOVSF3 instrument (WetLabs Inc; Moore et al., 2000) was used to measure scattering at three backscattering angles (100°, 125°, 150°) and three visible wavelengths (450, 530, 650 nm). Measurements were corrected for attenuation and were integrated (90-180°) to obtain the total backscattering coefficient according to manufacturer's instructions. Measurements by Boss et al. (2004) in the Case 2 waters off the coast of New Jersey showed that estimates of b_b using an ECOVSF3 instrument were in very good agreement (R^2=0.99) with b_b measurements using a HOBILabs Hydroscat-6 (Maffione and Dana, 1997). These results increase confidence on the accuracy of the backscattering measurements technique, especially since the instruments have large differences in design and calibration (Boss et al., 2004). Measurements of b_b were available only at wavelengths 450, 530, and 650 nm. As there are not enough data in the literature on the spectral dependence of b_b in the UV and near-infrared wavelengths for Chesapeake Bay, b_b was considered constant below 450 nm and above 650 nm in our RT modeling.

Two sensor arrays were used to measure underwater radiation fields in this work, depending on instrument availability. On 8 cruises we used Satlantic OCI-200 seven-channel irradiance sensors to measure the underwater upwelling, Eu(z), and downwelling, Ed(z), spectral irradiance profiles, as well as the above-water surface downwelling irradiance, Es, in the visible wavelengths. The irradiance sensors were mounted on a custom frame so that up- and down-welling sensors were nearly coplanar. On 7 cruises we used a Satlantic MicroPro free-falling radiometer (Table 1) to measure water column profiles of upwelling radiance, Lu(z), and Ed(z) in the water column, and Satlantic OCR-507 Surface Reference Irradiance sensors for

measurements of *E*s, at 14 wavebands (Table 2) . The MicroPro contains a pressure sensor that gives depth, and a miniature biaxial clinometer for tilt measurements (accuracy of 0.2^{o}) (Satlantic MicroPro operation manual, 2002).

When using the MicroPro, three casts were made at each station, and all casts were completed within 5-8 minutes. Casts characterized by large tilt-angles or changing cloudiness conditions were omitted from analysis. In cases when all *L*u(z) casts were of good quality, upwelling radiance was estimated as the average of three casts. A correction was applied to the radiometric measurements through the instrument's calibration for the immersion effect (Satlantic MicroPro operation manual, 2002). The upwelling radiance measurements were corrected for the depth offset between the *E*d and *L*u sensors.

Measurements of *L*u(z) were also corrected for self-shading (Gordon and Ding, 1992; Zibordi and Ferrari, 1995). According to Gordon and Ding (1992) and Zibordi and Ferrari (1995), the magnitude of instrument self-shading error depends mainly on the size of the radiometer, the solar zenith angle, and the total in-water absorption, and can be very significant in highly absorbing, coastal waters. However, field observations by Zibordi and Ferrari (1995) suggest that the presence of highly scattering material, as occurs in Chesapeake Bay, could reduce the self-shading error below that theoretically predicted based on the Gordon and Ding model. The MicroPro instrument, used in our measurements of *L*u(z), has a smaller diameter (6.4 cm) compared to other radiometric instruments and is less subject to instrument self-shading (Harding and Magnuson, 2002).

To estimate *L*w, we extrapolated underwater *L*u(z) measurements to just below the water surface $z=0^{-}$ and estimated transmittance through the water-air interface. On days when measurements were compared with the RT model (i.e. days when detailed *L*u and *E*d profiles

were measured), in situ IOPs were almost constant with depth over the first 3 m, and upwelling radiances decreased exponentially with depth at least down to 3-4 m. Therefore, $Lu(z)$ can be expressed as:

$$Lu(z,\lambda) = Lu(0^-,\lambda)\cdot \exp(-K_{Lu}\cdot z) \qquad (2)$$

where $Lu(0-,\lambda)$ is the upwelling radiance just beneath the water surface and K_{Lu} is the diffuse attenuation coefficient for the upwelling radiance. The upwelling radiance just below the water surface, $Lu(0-,\lambda)$ and K_{Lu} were estimated by non-linear least squares fitting of measured $Lu(z,\lambda)$ to Eq. 2 using the Marquardt-Levenberg algorithm (SigmaStat software). The coefficients of determination (R^2 values) for the non-linear exponential fits were in most cases better than 0.99. To estimate Lw, $Lu(0-,\lambda)$ was propagated through the water-air interface:

$$Lw(\lambda,\theta,\varphi) = Lu(0^-,\lambda,\theta',\varphi)\frac{(1-r(\theta',\theta))}{n_w^{\,2}} \qquad (3)$$

where θ' is the direction of the upward traveling photons incident from the water body onto the water surface, θ is the direction of the transmitted photons, $r(\theta',\theta)$ is the Fresnel reflectance for the associated directions θ' and θ, and n_w is the index of refraction of water ($n_w \approx 1.34$) (Mobley, 1994). For the geometry of our measurements, the zenith angle of water-leaving radiance and the nadir angle of in-water upward radiance are zero ($\theta'=\theta=0$) and the transmittance is ($1-r(\theta',\theta)\approx 0.98$. Therefore, $Lw(\lambda)$ can be estimated from Eq.(3), as:

$$Lw(\lambda) = 0.544\, Lu(0^-,\lambda) \qquad (4)$$

2.3 Laboratory measurements

Water samples were collected from discrete depths at the four stations for analysis of IOPs and water quality in the laboratory. We used filtration to partition absorption among particulate and dissolved components. Particulate material was collected on 25 mm glass fiber filters (Whatman GF/F), while the filtrate passing a 0.22 μm pore-diameter polycarbonate membrane filters was used to measure absorption by CDOM. Absorbance spectra of the filters and filtrate were measured using a Cary-IV dual-beam spectrophotometer to estimate the contribution of phytoplankton, non-algal particulate matter, and CDOM to the total light absorption, using the approach of Gallegos and Neale (2002). Absorption spectral slope coefficients describing the exponential decrease of absorption with increasing wavelength for CDOM, S_{CDOM}, and non-algal particulate matter, S_{nap}, were determined by applying non-linear exponential fits to the absorption coefficients vs wavelength (290-750 nm). Absorbance spectra of the filters were corrected for scattering errors using a path-length amplification factor estimated empirically by comparing particulate optical density measured on filters and in particle suspension (Mitchell et al., 2000). Measurements of the optical density of the particle suspension were made using the Cary-IV equipped with a 110 mm integrating sphere coated with polytetrafluoroethylene, by placing the sample at the center of the sphere to minimize scattering errors (Nelson and Prezelin, 1993; Babin and Stramski, 2002). Chlorophyll-a concentration, [chl-a], was measured spectrophotometrically on 90% acetone extracts of seston collected on 47 mm GF/F glass fiber filters (Jeffrey and Humphrey, 1975).

2.4 Radiative Transfer Modeling

We used the extensively validated Hydrolight underwater RT program (Mobley, 1988) to estimate water-leaving radiances and underwater radiation fields for the Chesapeake Bay. These calculations allowed us to examine the consistency between independently measured bio-optical quantities, for those cruises when detailed measurements of in-water IOPs, upwelling radiances, and downwelling irradiances (MicroPro measurements) were available (Table 1). Mobley (1994) has given a detailed description of the physical assumptions and mathematical calculations in the Hydrolight model.

The measured quantities used as inputs to perform model calculations included: (i) total irradiance incident on the water surface; (ii) profiles of total (minus pure water) absorption and attenuation at nine wavelengths in the visible (Table 2); (iii) profiles of total backscattering at three wavelengths in the visible (Table 2); (iv) observations of surface wind-speed for model estimations of water surface roughness (Cox and Munk, 1954; Mobley, 2002); (v) observations of cloudiness during in-situ measurements; (vi) solar zenith angle estimations, based on the exact time and location of the measurements.

The Pope and Fry (1997) absorption values for pure water and the Smith and Baker (1981) seawater scattering coefficients with the Rayleigh-like pure-water scattering phase function were used in our RT simulations. As the water at the four measurement sites in the Chesapeake Bay was quite turbid, and information on bottom reflectance was not available, the water column was assumed to be infinitely deep below the greatest depth of interest. RT model sensitivity studies in which we varied the bottom reflectance in the model showed that this assumption did not affect model estimates of water-leaving radiances (Tzortziou, 2004).

Raman scattering and CDOM and chlorophyll-a fluorescence were included in all model runs, except as indicated. Measurements of [chl-a] were used as inputs to estimate the chlorophyll-a fluorescence. Measurements of CDOM absorption, $a_{CDOM}(440)$, and S_{CDOM} were used as inputs in model estimations of CDOM fluorescence. Model runs were performed over a 350-700 nm wavelength range to include the relevant fluorescence excitation and emission wavelengths (Mobley and Sundman, 2000). In-situ measurements of fluorescence quantum yield were not performed in this study. Therefore, we used Hydrolight default assumptions for fluorescence efficiency and wavelength redistribution functions for fluorescence by chlorophyll (Mobley, 1994) and CDOM (Hawes, 1992).

We varied the option selected to represent backscattering within Hydrolight as part of our investigation. The widely used "Petzold average particle" VSF, with a backscattering fraction of 0.018, is available as a tabulated function within Hydrolight. We compared predictions using the Petzold average particle VSF with those using the more versatile Fournier-Forand (FF) VSF, also available as an option within Hydrolight (Mobley et al., 2002). The FF VSF is an analytical representation of the angular scattering of light that is determined by the particle index of refraction and the particle-size distribution (Fournier and Forand 1994). Mobley et al. (2002) demonstrated that the FF VSF can be specified mainly by the backscattering fraction, b_b/b, which we determined from our in situ measurements using the AC9 and ECOVSF3 instruments.

3. Results

A wide range of in-water optical characteristics, atmospheric, and air-water surface boundary conditions were observed in the mid-mesohaline Chesapeake Bay during our cruises. Relatively clear waters were observed during late fall months, while more turbid waters with higher total attenuation and absorption coefficients and higher [chl-a] values were observed during the spring-summer months (Tzortziou, 2004). The large variation in the measured IOPs and *E*s resulted in large spatial and temporal variations in the magnitude of measured water-leaving radiance, *L*w. However, in all cases, maximum values of *L*w occurred in the green wavelengths because of the high CDOM and non-algal particulate absorption in the blue and the high pure-water absorption in the red region of the spectrum.

This set of measurements formed the basis of an optical closure experiment that was used to examine particulate backscattering properties, long wavelength particulate absorption, and chlorophyll fluorescence characteristics. RT modeling was compared with measured bio-optical quantities for a total of 16 profiles (range of in-situ data shown in Table 3). Almost 85% of the IOP and [chl-a] values observed in the Chesapeake Bay during all our cruises were within the range of values for which RT model simulations were performed. In the next sections, we focus on measurements and model calculations of *E*d, *L*u, and *L*w for an example data set obtained at station PI on 28 September 2001. In-situ profiles of IOPs for this date are shown in Figure 3.

3.1 Backscattering properties

In-situ measurements of backscattering in the mid-mesohaline Bay showed large spatial and temporal variation, with surface $b_b(530)$ in the range 0.013 – 0.166 m^{-1}. Higher b_b values (by more than a factor of two in some cases) were observed consistently in the turbid water near

station JT. Considerable variation was also observed in the estimated backscattering fraction, with b_b/b values ranging from 0.006 to 0.036 at 530 nm. Large values were measured close to the bottom, consistent with an increase in the proportion of resuspended inorganic sediments relative to organic particles with depth. Particulate b_b/b at 530 nm had an average value of 0.0128 ±0.0032 (s.d.), considerably smaller than the Petzold average particle b_b/b of 0.018. Spectral dependence of b_b/b was weak, with average b_b/b equal to 0.0133±0.0032 at 450 nm and 0.0106±0.0029 at 650 nm.

We investigated the effect of the choice of VSF and the importance of variability in b_b magnitude and spectral shape for accurate RT modeling of Ed(z), Lu(z), and Lw, using the example dataset (measured b_b/b in the blue-green close to 0.015) (Figure 4, open diamonds). Assumption of a Petzold phase function in our model simulations led to an underestimation of Ed by ≅ 20% at 3-5 m depths compared to measurements. Lw was overestimated by 30% in the blue wavelengths and by 30-50% in the 550-650 nm wavelength region (Figure 4, stars). This large disagreement resulted mainly because the assumed b_b/b of 0.018 was too large for the specific waters.

The agreement between model simulations and measurements markedly improved when information on b_b/b magnitude was incorporated into the model by using a Fournier Forand (FF) phase function scaled to measured b_b/b profiles (Mobley et al., 2002). Use of a FF phase function with a backscattering fraction constant with wavelength and depth (b_b/b=0.015) resulted in an overestimation of Lw by ~15% at 490 nm because the measured b_b/b was close to 0.015 at the blue-green wavelengths. Overestimates were larger, ca. 20-30% at the red wavelengths because measured b_b/b showed a small decrease with increasing wavelength (Figure 4, filled circles).

Finally, modeling b_b using a FF phase function and accounting for the b_b/b spectral shape and vertical structure further improved the agreement between data and model simulations. Absolute percent differences between model estimated and measured $L_w(\lambda)$ were reduced to less than 10% at all wavebands (Figure 4, filled squares). Indeed, use of FF VSF constrained by measured wavelength- and depth-dependent backscattering fractions consistently improved agreement between model and data for all our cruises (results shown below). However, we observed a remaining tendency for the model to overestimate both L_u and E_d profiles, especially at the green wavelengths. We, therefore, considered whether systematic underestimation of absorption, $a_{t\text{-}w}$, could be responsible for this tendency toward overestimation at green wavelengths.

3.2 Absorption properties

Laboratory measurements of dissolved and particulate absorption showed that, although highly variable in concentration, CDOM and non-algal particles in the mid-mesohaline Chesapeake Bay contribute considerably to light attenuation in the short visible wavelengths. Their combined contribution to $a_{t\text{-}w}$ was on average 59% at 488 nm, and even larger at shorter wavelengths due to the exponential increase in absorption of both substances with decreasing wavelength. S_{nap} had an average value of 0.011 nm^{-1}, whereas average S_{CDOM} was 0.018 nm^{-1}.

An absorption spectral slope of 0.011 nm^{-1} for non-algal particulates implies that non-algal particulate absorption at 715 nm would be nearly 5% of its value at 440 nm. Measurements of particulate absorption spectra both for particulates on glass fiber filters (standard method) and for particle suspensions inside an integrating sphere showed low, but non-zero, absorption in the wavelength region 700-730 nm (example data shown in Figure 5). Measured $a_{t\text{-}w}(715)$ values for

the Bay were typically of the order of 0.03 m^{-1} (± 0.01 s.d.), commensurate with expectations based on S_{nap}.

Ramifications of this residual, long-wavelength, particulate absorption for estimation of radiometric quantities in the visible were examined more thoroughly for the example data set (Figure 6). For this case measured particulate absorption at 715 nm was close to 0.02 m^{-1} (Figure 5). Large differences between measured and model-estimated *L*u and *E*d profiles were observed at the green wavelengths (Figure 6, open circles) when model simulations were performed using as inputs AC9 data corrected assuming zero $a_{t\text{-}w}(715)$ (Eq. 1). Percent differences between model-estimated and measured *L*u values at 1 m depth were 17 % at 490 nm and 17.2% at 554 nm. The model overestimated both *E*d(z) and *L*u(z), and the disagreement between measurements and model estimations increased with increasing depth. Similar results were observed when comparing measurements and RT model estimations for other days and stations. The overestimation of both *L*u and *E*d by the model could not be explained only by errors in measured b_b, as overestimation, for example, of b_b would result in overestimation of *L*u but underestimation of *E*d.

When we ran the model allowing for non-zero particulate absorption at 715 nm when correcting in-situ measured absorption spectra, the agreement between measurements and model results was largely improved for both *L*u and *E*d (Figure 6, filled circles). In this case, a modified AC9-data correction for scattering errors was performed according to:

$$a_{t-w}(\lambda)_{corrected} = a_{t-w}(\lambda)_{measured} - \frac{a_{t-w}(715)_{measured} - a_{CARY}(715)}{b_{t-w}(715)_{measured}} b_{t-w}(\lambda)_{measured} \quad (5)$$

where $a_{CARY}(715)$ is the total (minus pure water) absorption at 715 nm measured spectrophotometrically. The effect that this correction had on total absorption, $a_t(\lambda)$, is shown in Figure 7. Maximum (more than 8%) percent differences were observed at the green wavelengths,

while the effect was relatively small in the blue and red regions of the spectrum. As a result, accounting for the residual particulate absorption at 715 nm had relatively larger effects on model estimates in the green wavelength region (Figure 6), while changes at blue and red wavelengths were marginal. Percent differences between model-estimated and measured Lu values at 1 m depth improved to 9% at 490 nm and 5.8% at 554 nm (compared with 17 % and 17.2%, respectively, without allowing for small positive $a_{t\text{-}w}(715)$). Similar improvement in the agreement between model and data was observed for the rest of our cruises.

3.3. Modeling fluorescence in the Chesapeake Bay

In addition to backscattering and absorption, fluorescence processes can significantly affect the magnitude and spectral shape of reflectance in coastal waters. For the example data set (measured [chl-a] of 7.3 mg m^{-3} and $a_{CDOM}(440)$ of 0.3 m^{-1}), model simulations of Lu(0^-) underestimated measured values in the 670-690 nm wavelength region by as much as 30-40% when chlorophyll-a fluorescence was neglected, compared to model results when fluorescence was included in the simulations. This underestimation of Lu(0^-) also resulted in an underestimation of Lw and Rrs at wavelengths close to the chlorophyll-a fluorescence emission maximum at 685 nm. Including chlorophyll fluorescence in our model simulations, using a fluorescence efficiency of 0.02, decreased the absolute percent differences between model-estimated and measured Lw to 8% at 670 nm and 4% at 684 nm, compared with 25% and 38% underestimates, respectively, when neglecting the chlorophyll fluorescence signal (Figure 8).

The model-estimated CDOM fluorescence signal affected underwater light fields only at wavelengths smaller than 530 nm (data not shown). For the specific case studied, neglecting

CDOM fluorescence in model estimations resulted in a 2-5% underestimation of *R*rs and *L*w values at the blue wavelengths, while the effect was negligible at longer wavelengths.

3.4 Overall RT model performance

To examine the overall RT model performance when properly accounting for the specific optical characteristics measured in the Chesapeake Bay, we performed model simulations of radiation fields for several selected cruises (Table 1), encompassing a wide range of water and boundary conditions (Table 3). Based on the foregoing results, which are summarized in Table 4, we: (i) used a FF phase function as determined by measured profiles of b_b/b spectra to account for the observed temporal and spatial variability of b_b/b, (ii) allowed for a small particulate absorption at the 715 nm wavelength region (equal to the measured $a_{CARY}(715)$) when correcting AC9 absorption estimates used as input to the model, and (iii) simulated chlorophyll-a fluorescence. For completeness, we also included fluorescence by CDOM, though neglecting CDOM fluorescence in RT model calculations had a relatively small effect on model estimations of *R*rs and *L*w.

The results of the comparisons between measured and model-estimated *E*d(z) and *L*u(z) are first shown (at wavelengths 443, 554, and 670 nm) for examples of relatively clear (28 September 2001, Figure 9, Table 5) and more turbid (22 May 2002, Figure 10, Table 5) waters. Model estimated quantities were in very good agreement with measurements in both cases, especially within the first three meters in the water column. For average values of attenuation ($c(412)$=5.5 m^{-1} and $c(532)$=4.2 m^{-1}) measured in the Bay during our cruises, the upper three meters correspond to optical depths ($\zeta = c\,z$) of 16.5 and 12.5, at wavelengths 412 and 532 nm, respectively. Correspondence between model-estimates and measurements in the two cases

shown in Figures 9 and 10 was similar to those for other days (Figures 11(a), 11(b)). Over all model runs, average absolute percent differences between model-estimated and measured Lu at 1 m depth below the water surface were 7.8% at 443 nm, 12.8% at 554 nm, and 8.7% at 670 nm. Average absolute percent differences between measured and model-estimated Ed at 1 m depth were 6.5% at 443 nm, 5.2% at 554 nm and 5.9% at 670 nm. In general, close agreement was found for all profiles, as shown in Figures 11(a) and (b), and measured by a coefficient of determination (R^2) between model and observed values. In the upper three meters (N=356) R^2 was 0.99 for Ed and 0.95 for Lu. For larger depths (N=315) estimated R^2 was smaller, 0.95 and 0.92 for Ed and Lu respectively.

Measured Lw spectra showed considerable variation in magnitude among cruises and stations, reflecting the observed variation in IOPs and Es (Figure 12). Despite this variability, in-situ measurements of Lw(λ) were in very good agreement with model estimates in all cases (Figure 12, Table 6). Average absolute percent differences between measured and model-estimated Lw(λ) were on the order of 6.35% at 443 nm, 7.73% at 554 nm and 6.86% at 670 nm (Table 6, last row). The magnitude and direction of the percent differences between data and model results did not show any seasonal or spatial patterns (e.g. more- versus less-turbid waters). There was not any strong tendency by the model to overestimate or underestimate Lw in the 412-670 nm wavelength region. On average, there was a slight model overestimation of Lw in the green wavelengths, but this was smaller than the standard deviation of differences between modeled and observed Lw. Although including chlorophyll fluorescence in our RT modeling largely improved agreement between model and data, in most of the cases the model still overestimated Lw at 685 nm (average absolute difference close to 13%, Table 6).

4. Discussion

Effective interpretation of ocean color in estuarine and coastal waters requires accurate modeling of bio-optical processes based on *in-situ* information. Therefore, successful remote retrieval of biogeochemical variables in near-shore waters depends largely on the accuracy of, and consistency among, the in-situ bio-optical data used in the development, validation, and regional optimization of the applied ocean-color algorithms. It is in this sense that using RT to evaluate the validity of any modeling assumptions, and examine the degree of closure among bio-optical quantities independently measured at the field, becomes critical for remote sensing applications (Figure 1). In this paper, we used new, in-situ bio-optical data for the Chesapeake Bay combined with RT closure results to: (i) examine the effect of backscattering variability, non-algal particulate absorption characteristics, and chlorophyll fluorescence properties on *R*rs retrievals for these optically thick estuarine waters, and (ii) evaluate the overall consistency between measured IOPs and resulting radiation fields as a step towards applying data and RT model results to the analysis of remotely-sensed ocean color in the mid-measohaline Chesapeake Bay.

Backscattering processes in coastal waters strongly influence the magnitude of radiance leaving the water surface and eventually measured by a remote sensing instrument. Particulate backscattering in the mid-Chesapeake Bay showed considerable variability, depending on particulate loading, distance from land, and mixing processes. Measured backscattering fractions had an average value of 0.0128 at 530 nm, in agreement with b_b/b values reported in studies of coastal waters off Mississippi (Sydor and Arnone, 1997) and New Jersey (Mobley et al., 2002; Boss et al., 2004). The observed spectral shape of b_b/b is in agreement with Mobley et al. (2002), who measured a weak, b_b/b wavelength dependence, with a decrease in b_b/b from 442 to 555 nm

by less than 24 %, in the Case 2 waters offshore of New Jersey. Spatial and temporal variations in surface particulate backscattering in the Bay were strongly correlated to spatial and temporal patterns of surface non-algal particulate absorption (Tzortziou 2004). Higher b_b values (by more than a factor of two in some cases) were observed consistently in the turbid water near station JT. This station is located closest to the land, is the shallowest among the four stations, and is more strongly influenced by bottom resuspension and shoreline erosion (Figure 2). These results, and the much smaller correlation found between particulate b_b and [chl-a], indicate that highly refractive non-algal particles, such as minerals or detrital material of relatively low water content, are the major water constituents regulating b_b variability in the mid-mesohaline Chesapeake Bay (Tzortziou 2004). This information on backscattering characteristics could improve remote retrievals for the Chesapeake Bay, through the development of new backscattering parameterizations and regional-specific algorithms that relate *R*rs to backscattering magnitude and concentration of non-algal suspended particles.

Magnuson et al. (2004) recently examined the parameterization and validation of the semi-analytical, bio-optical Garver-Siegel-Maritorena model (i.e. GSM01, Maritorena et al., 2002) for application in the Mid-Atlantic Bight and Chesapeake Bay. According to their results, the lack of direct measurements of backscattering in the Chesapeake Bay significantly affected backscattering parameterization as well as the evaluation of the model's backscattering product. Because of the lack of backscattering data, Magnuson et al. estimated b_b from total scattering, b, assuming a constant b_b/b of 0.018 (from Petzold data). This approach resulted in an overestimation of b_b compared to the b_b product of the GSM01-CB model (i.e. the GSM01 model tuned for the Chesapeake Bay). Magnuson et al. reduced the bias between estimated and

model b_b for the Chesapeake Bay waters (their figures 11(g), 11(h)) by using a b_b/b of 0.0125, close to our mean value for surface $b_b/b(530)$).

Our RT model simulations showed that the Petzold 'average particle' assumption is usually not applicable for the mid-mesohaline Chesapeake Bay. As measured backscattering fractions in these waters had an average value of 0.0128 at 530 nm, use of the Petzold VSF with a b_b/b of 0.018 overestimated backscattered radiation compared to most observations. We obtained the best agreement between model-simulated and measured radiation fields when we modeled particulate backscattering using a FF scattering phase function as determined by measured wavelength- and depth-dependent backscattering fractions (Figure 4, Table 4). These results are in agreement with studies by Mobley et al. (2002) for the near shore waters off the coast of New Jersey (b_b/b within the range 0.004-0.015). The use of a FF scattering phase function constrained by measured b_b/b allowed us to incorporate information on b_b/b magnitude, spectral shape, and vertical structure into the RT model, and account for the b_b/b spatial and temporal variability observed in the Bay waters. Chang et al. (2003) performed an optical closure experiment in the near shore waters off New Jersey, in which RT model simulations were run using measured VSFs constant with wavelength and depth. Their average absolute percent differences between measured and model-estimated $Lw(\lambda)$ were of the order of 20% at 443 nm, 22% at 554 nm, and 17% at 682 nm, similar to the results we obtained when using vertically and spectrally constant b_b/b (Table 4). By using measured, vertically and spectrally resolved, profiles of b_b/b, we obtained absolute percent differences between measured and model-estimated Lw smaller than 10% at all wavebands, improving optical closure in coastal waters. Therefore, detailed information on backscattering variability, including vertical and spectral resolution of

backscattering processes, is necessary for RT modeling of water reflectance in the Chesapeake Bay and application of both data and model results to remote sensing algorithm development.

One common assumption when correcting in-situ AC9-data for scattering errors is that particulate absorption at 715 nm is zero (Zaneveld et al., 1994). In contrast, our measurements in the mid-mesohaline Chesapeake Bay revealed small, non-zero particulate absorption in the wavelength region 700-730 nm. This low absorption is consistent with the gradual, exponential decrease of the non-algal particulate absorption with increasing wavelength (average $S_{nap} = 0.011$ nm^{-1}). Weak particulate absorption in the 700-730 nm was also shown by Gallegos and Neale (2002) for the Rhode River sub-estuary on the western shore of the mesohaline Chesapeake Bay, and by Tassan and Ferrari (2003), Babin and Stramski (2002), and Babin et al. (2003) for other coastal waters.

Our model simulations showed that accounting for the small particulate absorption at 715 nm, when processing in-situ measured AC9 data (modified AC-9 correction according to equation 5), further improved RT closure in the Bay waters by reducing the model's systematic overestimation of both *E*d and *L*u. Due to strong absorption by CDOM and non-algal particulates at blue wavelengths, and water itself at red wavelengths, the effect was most noticeable at green wavelengths (i.e. 554 nm). In this wavelength region total absorption is relatively smaller, and a small change in the absorption, equal to the weak particulate absorption at 715 nm, had a relatively larger effect on model simulations (Figures 6, 7). Failure to account for the small near-infrared particulate absorption when defining inputs for the RT model therefore, leads to consistent, though variable, model overestimation of *R*rs around 554 nm. This is a key wavelength region that is being used in both empirical and semi-analytical satellite

algorithms for remote chlorophyll retrievals (e.g. O' Reilly et al., 2000, Maritorena et al., 2002, Carder et al., 1999).

As fluorescence is an indicator of both the amount of chlorophyll and the rate of photosynthesis much attention has been focused on the use of remotely sensed chlorophyll fluorescence signal for inferring information on primary productivity and phytoplankton physiological state in coastal waters (e.g. Gower et al., 1981, Abbot and Letelier 1999; Huot et al., 2005). Accounting for chlorophyll fluorescence in our RT model simulations for the mid-mesohaline Chesapeake Bay removed large errors in modeling *R*rs at the red wavelengths. Neglecting chlorophyll fluorescence for a chlorophyll concentration of 7.3 mg m^{-3} resulted to model underestimations of *L*w and *R*rs by 30-40% in the wavelength region around the chlorophyll fluorescence maximum compared to our data. Including chlorophyll fluorescence in our RT modeling of the example station considerably improved agreement between model and data reducing absolute percent differences to 4-8% (Figure 8, Table 4). A tendency by the RT model to overestimate *L*w at 685 nm could result from an overestimate of chlorophyll fluorescence efficiency for these near-surface waters. In-situ measurements by Maritorena et al. (2000) in the case 1, oligotrophic to eutrophic Pacific waters, showed that vertical profiles of fluorescence quantum yield were strongly structured, with maximal (5–6%) values at depth, and relatively low (1%) values closer to the surface, due to photoinhibition. Similar *in-situ* determinations of chlorophyll fluorescence efficiency variability for the Chesapeake Bay waters would further improve model estimates of reflectance at red wavelengths. However, even with a constant fluorescence efficiency (2%), our average overestimation of *L*w at 685 nm was less than 13% over all stations (Table 6). These results suggest that remote retrieval of chlorophyll fluorescence may provide a better basis for satellite monitoring of phytoplankton in these Case 2

waters compared to *R*rs in the blue and green where absorption is dominated by CDOM and non-algal particles.

When we applied the results from our measurements to model bio-optical processes in the complex Chesapeake Bay estuarine waters, we obtained very good optical closure between independently measured IOPs and radiation fields over the wide range of observed bio-optical conditions. Model *E*d and *L*u values, estimated from measured IOPs, were in good agreement with measurements (Figures 9, 10, 11) especially within the first three meters that, in these optically thick waters, are the most important for remote sensing. The agreement between model and data extended for over three orders of magnitude dynamic range in radiation fields. In the upper 3 m, coefficients of determination between model and observed values were 0.99 and 0.95 for *E*d and *L*u respectively. Closer to the bottom, larger percent differences between model and data typically occur in such optically thick waters, since both measurements and model results have relatively high levels of uncertainties due to very low light levels and small model-input errors that propagate in the RT model calculations.

Although there was a wide range in the magnitude of measured *L*w spectra, reflecting variation in *E*s and water IOPs, *L*w(λ) measurements were consistently in good agreement with model results. The magnitude and direction of the percent differences between model and data did not depend on season or location (more- versus less-turbid waters). There was not any strong tendency by the model to overestimate or underestimate *L*w in the 412-670 nm wavelength region. Average absolute percent differences between measured and model-estimated *L*w values were smaller than 10% in the 412-670 nm wavelength region (Figure 12, Table 6). These percent differences were considerably smaller than those presented in the few studies of optical closure performed previously in near shore waters of similar optical complexity (e.g. Chang et al., 2003;

Bulgarelli et al., 2003). The improved optical closure presented in this study was obtained after using depth and wavelength resolved measurements of b_b/b, properly correcting absorption measurements in a way that allowed a small residual particulate absorption at 715 nm, and including chlorophyll fluorescence in our model simulations. Given that our average values for b_b/b (Mobley et al., 2002; Boss et al., 2004) and S_{nap} (e.g. Roesler et al., 1989; Babin et al., 2003; Magnuson et al., 2004) were within the range of values reported in previous studies, and that our chlorophyll concentrations were not excessively high for estuaries, we expect that proper accounting for these optical characteristics would be equally important in optical modeling of other coastal and estuarine waters.

In summary, our study has shown that systematic comparisons between field observations and RT model simulations are useful for improving our knowledge of the optical characteristics (e.g. b_b, b_b/b, a), as well as the importance of certain processes (e.g. CDOM and chlorophyll-a fluorescence), in the optically complex and biologically productive Chesapeake Bay waters. It also suggests that the RT model used in this study can be used to estimate underwater and emergent radiation fields, even in waters characterized by high optical complexity, as long as accurate input data are available and the validity of the model assumptions is examined. The demonstration of good closure between independently measured radiation fields and water IOPs using RT modeling increases confidence in the accuracy of, and consistency among the in-situ data. Obtaining closure to this degree is a critical step towards applying bio-optical data and RT model results to the interpretation and validation of remotely sensed ocean color, i.e. the development, parameterization, and refinement of bio-optical algorithms for effective remote retrievals of biogeochemical quantities in the Chesapeake Bay.

Acknowledgements

Funds for this work were provided by NASA-Goddard Space Flight Center, the University of Maryland, and the Smithsonian Pre-doctoral Fellowship program. Field work in Chesapeake Bay was funded in part by the Coastal Intensive Site Network (CISNet) program of the United States Environmental Protection Agency through grant R826943-01-0. We thank K. Yee, D. Sparks, M. Mallonee and S. Benson for assistance in the field and laboratory.

References

Abbott M. R., and Letelier R. M., 1999, Chlorophyll Fluorescence (MODIS Product Number 20), MODIS Algorithm Theoretical Basis Document, ATBD-MOD-22, Version 3

Babin M., and Stramski D., 2002, Light absorption by aquatic particles in the near-infrared spectral region, *Limnology and Oceanography, Notes*, 47(3), 911-915

Babin M., Stramski D., Ferrari G., Clauster H., Bricaud A., Obelensky G., and Hoepffner N., 2003, Variations in the light absorption coefficients of phytoplankton, nonalgal particles, and dissolved organic matter in coastal waters around Europe, *Journal of Geophysical Research*, Vol. 108, N. C7, 3211

Boss E., Pegau W. S., Lee M., Twardowski M. S., Shybanov E., Korotaev G., and Baratange F., 2004, The particulate backscattering ratio at LEO 15 and its use to study particles composition and distribution. *Journal of Geophysical Research*, 109, C01014, doi:10.1029/2002JC001514

Bulgarelli B., Zibordi G., and Berthon J.F., 2003, Measured and modeled radiometric quantities in coastal waters: toward a closure, *Applied Optics*, 42(27), 5365-5381

Carder K., Stewart R., Harvey G., and Ortner P., 1989, Marine humic and fulvic acids: Their effects on remote sensing of ocean chlorophyll, *Limnology and Oceanography*, 34(1), 68-81.

Carder K. L., Chen F. R., Lee Z. P., and Hawes S. K., 1999, Semianalytical moderate-resolution imaging spectrometer algorithms for chlorophyll a and absorption with bio-optical domains based on nitrate-depletion temperatures, *Journal of Geophysical Research*, 104, 5403–5421

Chang G. C., Dickey T. D., Mobley C. D., Boss E., and Pegau W. S., 2003, Toward closure of upwelling radiance in costal waters, *Applied Optics*, 42(9), 1574-1582

Cox, C. and W. Munk, 1954, Statistics of the sea surface derived from sun glitter, *Journal of Marine Research.*, 13, 198-227

Fournier G. R., and Forand, J. L., 1994, Analytical phase function for ocean water, in *Ocean Optics XII*, J.S. Jaffe, ed. (SPIE - International Society for Optical Engineering Vol. 2258, 1994), 194-201.

Gallegos C. L., and Neale P. J., 2002, Partitioning spectral absorption in case 2 waters: Discrimination of dissolved and particulate components, *Applied Optics*, 41, 4220-4233

Garver S. A., and Siegel D. A., 1997, Inherent optical property inversion of ocean color spectra and its biogeochemical interpretation. I. Time series from the Sargasso Sea, *Journal of Geophysical Research*, 102, 18607–18625

Gordon H. R., 1979, Diffuse reflectance of the ocean: the theory of its augmentation by chlorophyll *a* fluorescence at 685 nm, *Applied Optics*, 18, 1161–1166

Gordon H. R., and Ding K., 1992, Self-shading of in-water optical instruments, *Limnology and Oceanography,* 37, 491-500

Gower, J.F.R., and Borstad G.A., 1981, Use of in vivo fluorescence line at 685 nm for remote sensing surveys of surface chlorophyll a, in *Oceanography from Space*, edited by J.F.R. Gower, pp. 329-338, Plenum, NY

Gower, J.F.R., 1980, Observations of in situ fluorescence of chlorophyll *a* in Saanich Inlet, *Boundary Layer Meteorol*ogy, 18: 235-245.

Harding Jr. L. W., and Magnuson A., 2002, Bio-Optical and Remote Sensing Observations in Chesapeake Bay, in *SIMBIOS Project 2001 Annual Report*, G. S. Fargion and C. R. McClain, eds. (NASA/TM, 2002), 52-62.

Harding Jr. L.W., Magnuson A., Mallonee M.E., 2005, Bio-optical and remote sensing observations in Chesapeake Bay, *Estuarine, Coastal and Shelf Science*, 62, 75-94

Hawes S. K., 1992, Quantum fluorescence efficiencies of marine fulvic and humic acids, *Master's Thesis*, Dept. of Marine Sc. Univ. of South Florida, St. Petersburg, FL

Huot Y., Brown C. A., and Cullen J.J, 2005, New algorithms for MODIS sun-induced chlorophyll fluorescence and a comparison with present data products, *Limnology and Oceanography: Methods*, 3, 108–130

Jeffrey S. W., and Humphrey G. F., 1975, New spectrophotometric equations for determining chlorophyll a, b, c, and c2 in higher plants algae and natural phytoplankton, *Biochemie and Physiologie der Pflanzen*, 167, 191-194

Kirk, J. T. O., 1992, Monte Carlo modeling of the performance of the reflective tube absorption meter, *Applied Optics*, 31, 6463-6468

Maffione, R. A., and Dana D. R, 1997, Instruments and methods for measuring the backward-scattering coefficient of ocean waters, *Applied Optics*, 36, 6057– 6067

Magnuson A., Harding L. W., Mallonee M. E., Adolf J. E., 2004, Bio-optical model for Chesapeake Bay and the middle Atlantic bight, *Estuarine, Coastal and Shelf Science,* 61, 403-424

Maritorena S., Morel A., and Gentili B., 2000, Determination of the fluorescence quantum yield by oceanic phytoplankton in their natural habitat, *Applied Optics*, 39, 6725-6737

Maritorena S., Siegel D. A., and Peterson A. R., 2002, Optimization of a semianalytical ocean color model for global-scale applications", *Applied Optics*, 41, 2705-2714

Mitchell G., Bricaud A., Carder K., Cleveland J., Ferrari G., Gould R., Kahru M., Kishino M., Maske H., Moisan T., Moore L., Nelson N., Phinney D., Reynolds R., Sossik H., Stramski D., Tassan S., Trees C. C., Weidemann A., Wieland J., and Vodacek A., 2000, Determination of spectral absorption coefficients of particles, dissolved material and phytoplankton for discrete water samples, in *Ocean Optics Protocols For Satellite Ocean Color Sensor*

Validation, Revision 2, G. S. Fargion and J. L. Mueller, NASA/TM-2000-209966, Chapter 12

Mobley C. D., 1988, A numerical model for the computation of radiance distribution in natural waters with wind-roughened surfaces, part II; user's guide and code listing", *NOAA Tech. Memo ERL PMEL-81* (NTIS PB88-246871) (Pacific Marine Environmental Laboratory, Seattle, Wash.)

Mobley C. D., 1994, Light and Water: Radiative Transfer in Natural Waters (Academic Press, San Diego, Calif., 1994).

Mobley C. D., 2002, Hydrolight Technical Note 1: How well does Hydrolight simulate wind-blown sea surfaces?, (Sequoia Scientific, Inc. 2002).

Mobley C. D., and Sundman L. K., 2000, Hydrolight 4.1-Users Guide (Sequoia Scientific, Inc., 2000).

Mobley C. D., Sundman L. K., and Boss E., 2002, Phase function effects on oceanic light fields, *Applied Optics*, 41, 1035-1050

Moore, C., Twardowski M.S., and Zaneveld J.R.V., 2000, The ECO VSF – A multi-angle scattering sensor for determination of the volume scattering function in the backward direction. *Proceedings from Ocean Optics XV*, October 16-20, Monaco

Morel A., and Prieur L., 1977, Analysis of variations in ocean color, *Limnology and Oceanography,* 22, 709-722.

Nelson, N. B. and Prezelin B. B., 1993, Calibration of an integrating sphere for determining the absorption coefficient of scattering suspensions, *Applied Optics*, 32, 6710-6717.

O'Reilly, J.E., Maritorena, S., Siegel, D., O'Brien, M.C., Toole, D., Mitchell, B.G., Kahru, M., Chavez, F.P., Strutton, P., Cota, G., Hooker, S. B., McClain, C.R., Carder, K.L., Muller-Karger, F., Harding, L., Magnuson, A., Phinney, D., Moore, G.F., Aiken, J., Arrigo, K.R., Letelier, R., and Culver, M., 2000, Ocean color chlorophyll a algorithms for SeaWiFS, OC2, and OC4: Version 4. *In: SeaWiFS Postlaunch Technical Report Series, edited by Hooker,*

S.B and Firestone, E.R. Volume 11, SeaWiFS Postlaunch Calibration and Validation Analyses, Part 3. NASA, Goddard Space Flight Center, Greenbelt, Maryland. 9-23.

Pegau, W. S., Gray, D., Zaneveld, J. R. V., 1997, Absorption and attenuation of visible and near-infrared light in water: dependence on temperature and salinity. *Applied Optics* 36, 6035 - 6046.

Petzold T. J., 1972, Volume scattering functions for selected ocean waters, SIO Ref. 72-78, (Scripps Inst. Of Oceanography, Visibility Laboratory, La Jolla

Pope R. M., and Fry E. S., 1997, Absorption spectrum (380-700 nm) of pure water. II. Integrating measurements, *Applied Optics*, 36, 8710-8723

Roesler, C. S., Perry M. J., and Carder K. L., 1989, Modeling in situ phytoplankton absorption from total absorption spectra in productive inland marine waters, *Limnology and Oceanography*, 34(8), 1510.

Satlantic, 2002, Operation Manual for the MicroPro, Revision D, June 2002

Smith R. C., and Baker K. S., 1981, Optical properties of the clearest natural waters (200-800 nm), *Applied Optics*, 20, 177-184

Sydor, M., Arnone, R.A., 1997, Effect of suspended particulate and dissolved organic matter on remote sensing of coastal and riverine waters, *Applied Optics 36,* 6905–6912.

Tassan, S., 1988, The effect of dissolved "yellow substance" on the quantitative retrieval of chlorophyll and total suspended sediment concentrations from remote measurements of water colour, *International Journal of Remote Sensing,* 9, 787–797.

Tassan S., and Ferrari G. M., 2003, Variability of light absorption by aquatic particles in the near-infrared spectral region, *Applied Optics*, 42, 4802-4810

Tzortziou M., 2004, Measurements and characterization of optical properties in the Chesapeake Bay's estuarine waters, using in-situ measurements, MODIS satellite observations and radiative transfer modelling", *PhD-Dissertation*, Dept of Meteorology, Univ. of Maryland, College Park, MD

Zaneveld J. R. V., Kitchen J. C., and Moore C., 1994, The scattering error correction of reflecting-tube absorption meters, in *Ocean Optics XII*, J.S. Jaffe, ed. (SPIE - International Society for Optical Engineering Vol. 2258, 1994), 44-55.

Zibordi G., and Ferrari G. M., 1995, Instrument self-shading in underwater optical measurements: experimental data, *Applied Optics*, 34, 2750-2754

Figure Legends:

Figure 1: 'Optical closure' and its role in the interpretation of ocean color observations in coastal waters. In the optical closure experiment, measurements of water optical characteristics (e.g. absorption, scattering, [chl-a]) are used as input information to perform theoretical RT model calculations for underwater and emergent radiation fields. Radiance and irradiance measurements can then be compared to the theoretically estimated radiometric quantities (model output). Depending on the results of the closure experiment, bio-optical data and model results can then be used to investigate errors in measurement methodology and uncertainties in model assumptions, and once good optical closure is achieved, they can be applied to the interpretation and validation of satellite observations, and the development, parameterization, and refinement of bio-optical models for regionally-specific, remote sensing ocean-color algorithms.

Figure 2: Location of in-situ measurements (stations HB, PI, TI and JT) and cruise track. The starting point was the SERC dock located in the Rhode River sub-estuary, along the western shore of the Chesapeake Bay.

Figure 3: Dataset collected from station PI on 28 September 2001. (a) temperature, T; (b) salinity, S; (c) absorption, $a_{t\text{-}w}$, at 440 nm (diamonds), 532 nm (squares), and 676 nm (circles); (d) attenuation, $c_{t\text{-}w}$, at 440 nm (diamonds), at 532 nm (squares), and 676 nm (circles); (e) backscattering, b_b, at 450 nm (diamonds), 530 nm (squares), and 650 nm (circles); (f) estimated backscattering fraction, b_b/b, at 450 nm (diamonds), 530 nm (squares), and 650 nm (circles).

Figure 4: Lw spectra estimated using three different b_b/b ratios (measured Lw are shown as open diamonds) and percent differences in Lw between measurements and model estimations using: (i) a Petzold "average particle" phase function (stars), (ii) a FF scattering phase function with a constant backscattering ratio, b_b/b=0.015 (filled circles); and (iii) a FF scattering phase function as determined by measured wavelength- and depth- dependent b_b/b

(filled squares). Percent differences in Lw between measurements and model estimations are shown in the inset figure (percent differences estimated as $(Lw_{model}-Lw_{data})/Lw_{data}$).

Figure 5: Particulate absorption (sum of absorption by phytoplankton and non-algal particles) in the 290-750 nm wavelength region, measured spectrophotometrically for station PI, on 28 September 2001. The residual non-zero particulate absorption at 715 nm is shown more clearly in the inset figure.

Figure 6: (Left column) Comparison between measured (solid lines) and model-estimated $Lu(z)$ (in $\mu Wnm^{-1}cm^{-2}sr^{-1}$) at 443, 554 and 670 nm, assuming $a_{t\text{-}w}(715)=0$ (open circles) and assuming $a_{t\text{-}w}(715)=a_{CARY}(715)$ (filled circles). (Right column) Similarly for $Ed(z)$ (in $\mu Wnm^{-1}cm^{-2}$). Data is shown for measurements performed at station PI, on 28 September 2001.

Figure 7: The effect of accounting for the residual particulate absorption at 715 nm on total absorption, $a_t(\lambda)$. The results are shown for measurements performed at station PI, on 28 September 2001 when measured particulate absorption at 715 nm was close to 0.02 m^{-1}.

Figure 8: Lw spectra estimated by the model, including (open circles) and neglecting (filled circles) chlorophyll-a fluorescence. Measured Lw are shown as open diamonds. Percent differences in Lw between measurements and model estimations are shown in the inset figure (percent differences estimated as $(Lw_{model}-Lw_{data})/Lw_{data}$).

Figure 9: (a) Model estimated $Lu(z)$ (in $\mu W\ nm^{-1}\ cm^{-2}\ sr^{-1}$) (open circles), at wavelengths 443, 554, 670 nm, are compared with in-situ measurements (solid lines) performed on 28 September 2001, as an example of the degree of closure obtained during a day when relatively clear water conditions were observed in the northern Bay. (b) Similarly, for $Ed(z)$ (in $\mu Wnm^{-1}cm^{-2}$). Percent differences between model-estimated and measured quantities at 1 m depth are given in table 5.

Figure 10: Same as figure 9, but for 22 May 2002, as an example of the degree of closure obtained during a day when highly turbid water conditions were observed in the Bay.

Figure 11: Comparison between model-estimated and in-situ measured (a) $Ed(z)$ (in $\mu Wnm^{-1}cm^{-2}$) and (b) $Lu(z)$ values (in $\mu Wnm^{-1}cm^{-2}sr^{-1}$) at depths 0-6m, for all cruises-stations that comparisons with the RT model were performed. Comparisons within the first 3 meters are shown as dark circles (R^2=0.99 for Ed, R^2=0.95 for Lu), while comparisons for depths below 3 m are shown as open circles (R^2=0.95 for Ed, R^2=0.92 for Lu), (the 1:1 line is also shown for comparison).

Figure 12: Water-leaving radiances, Lw, measured in-situ (open circles) and estimated by the model (solid line, filled diamonds), for measurements performed during our cruises in the Chesapeake Bay.

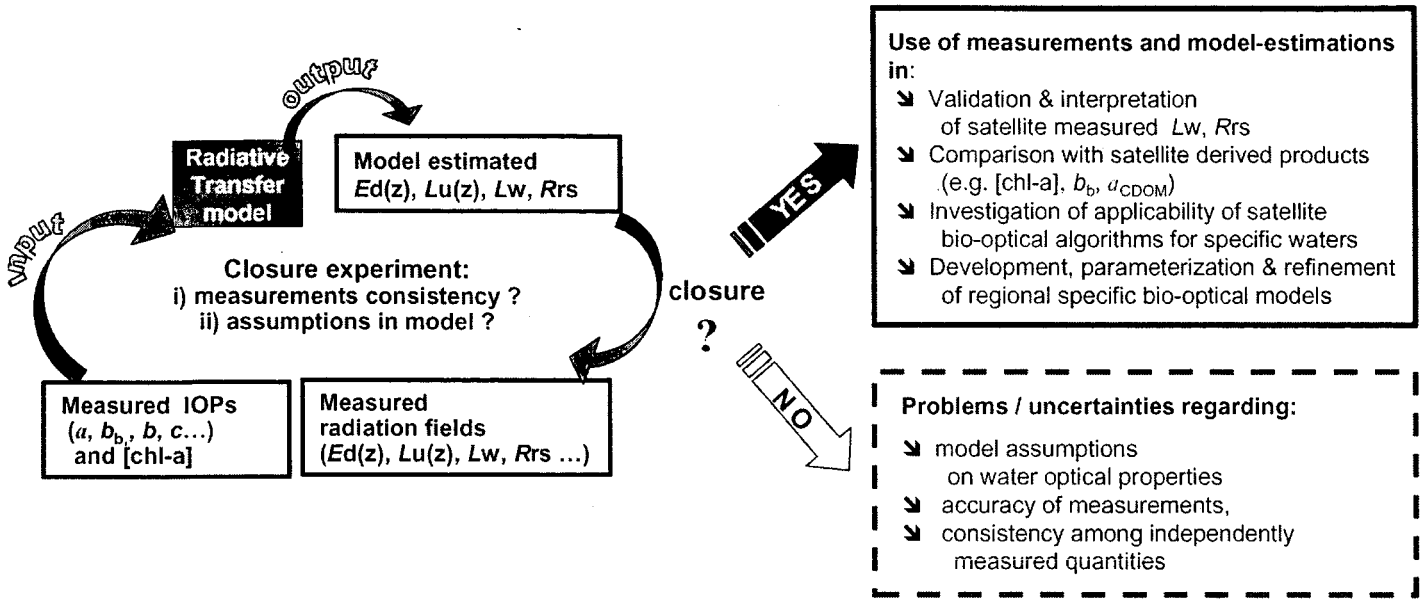

Figure 1, Tzortziou et al.,

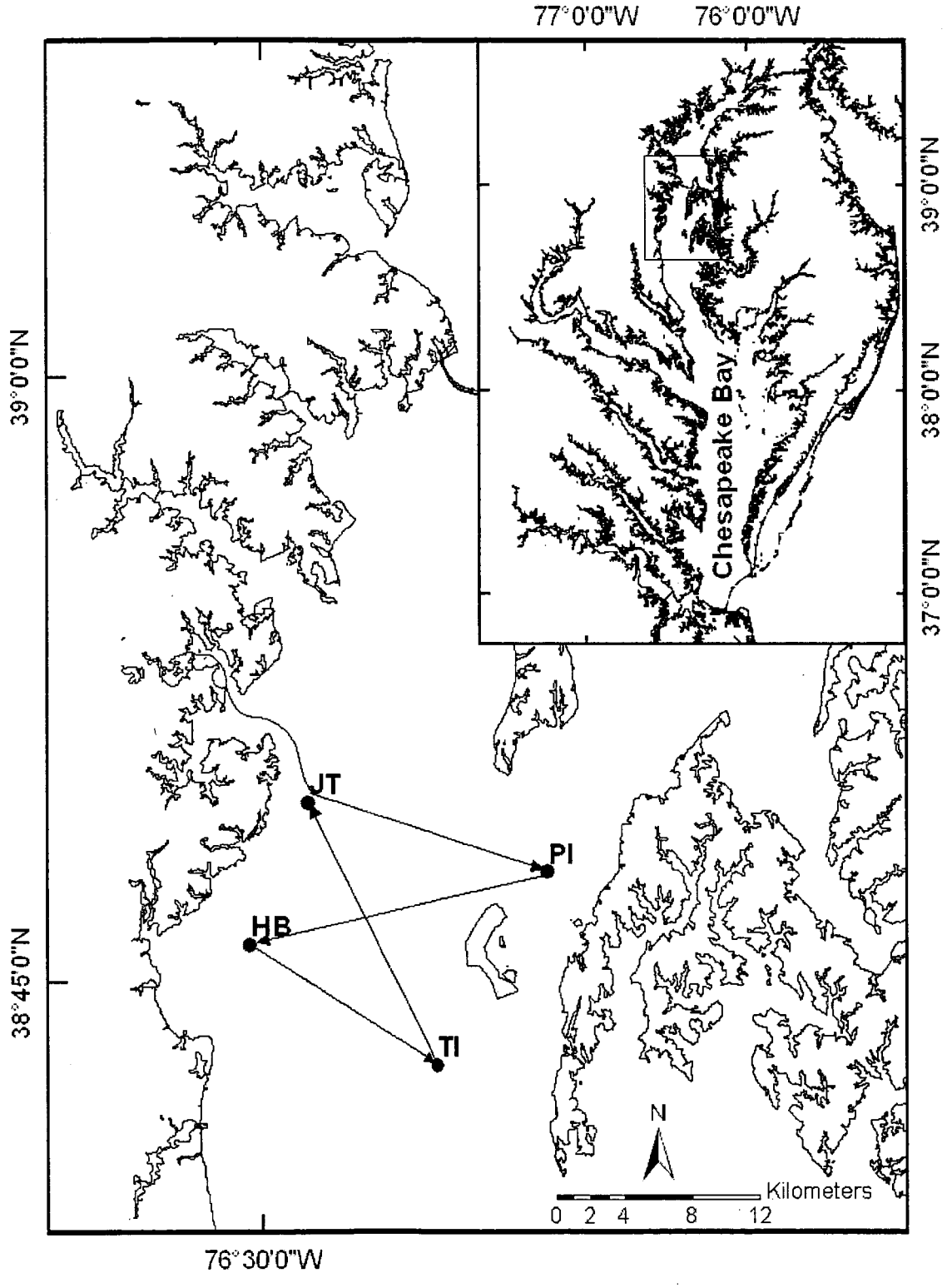

Figure 2, Tzortziou et al.,

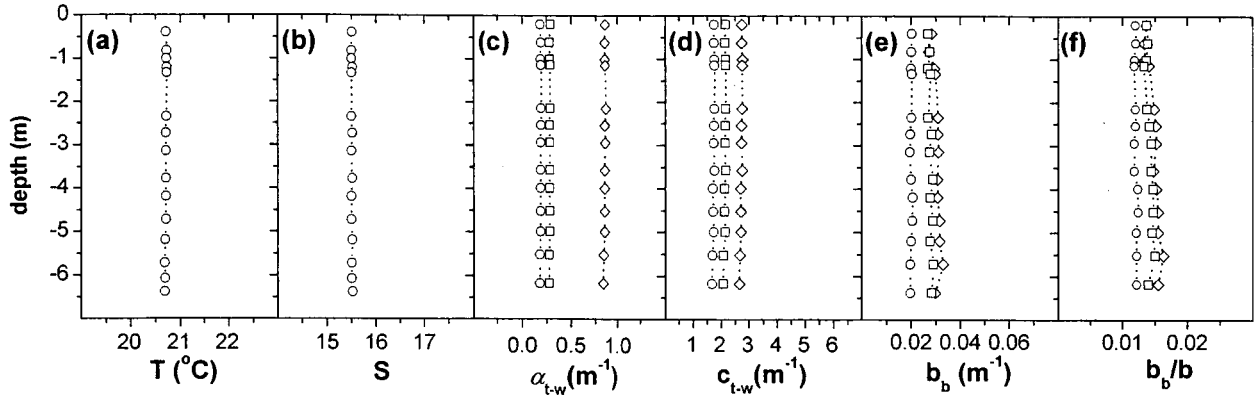

Figure 3, Tzortziou et al.,

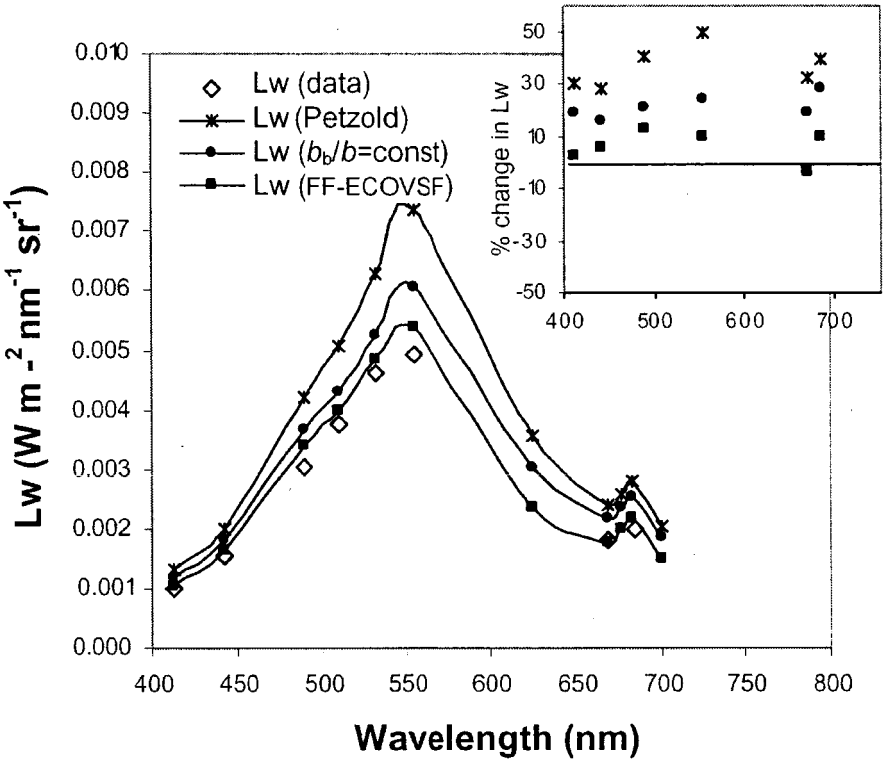

Figure 4, Tzortziou et al.,

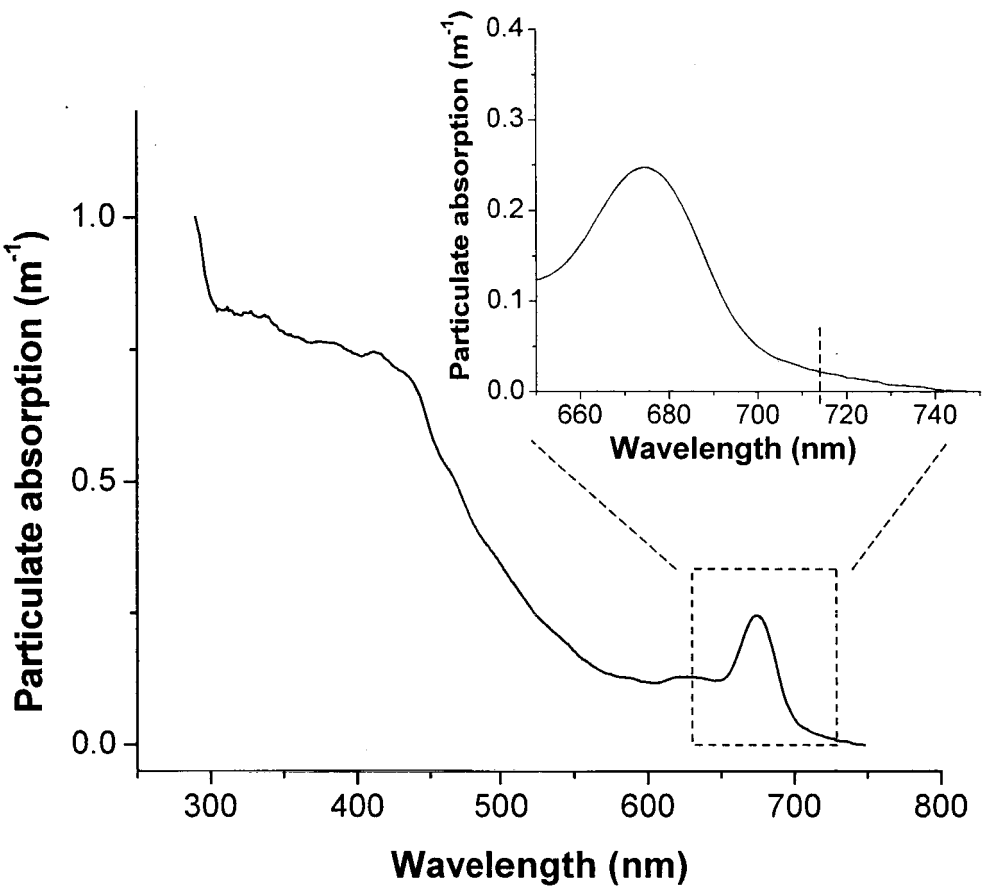

Figure 5, Tzortziou et al.,

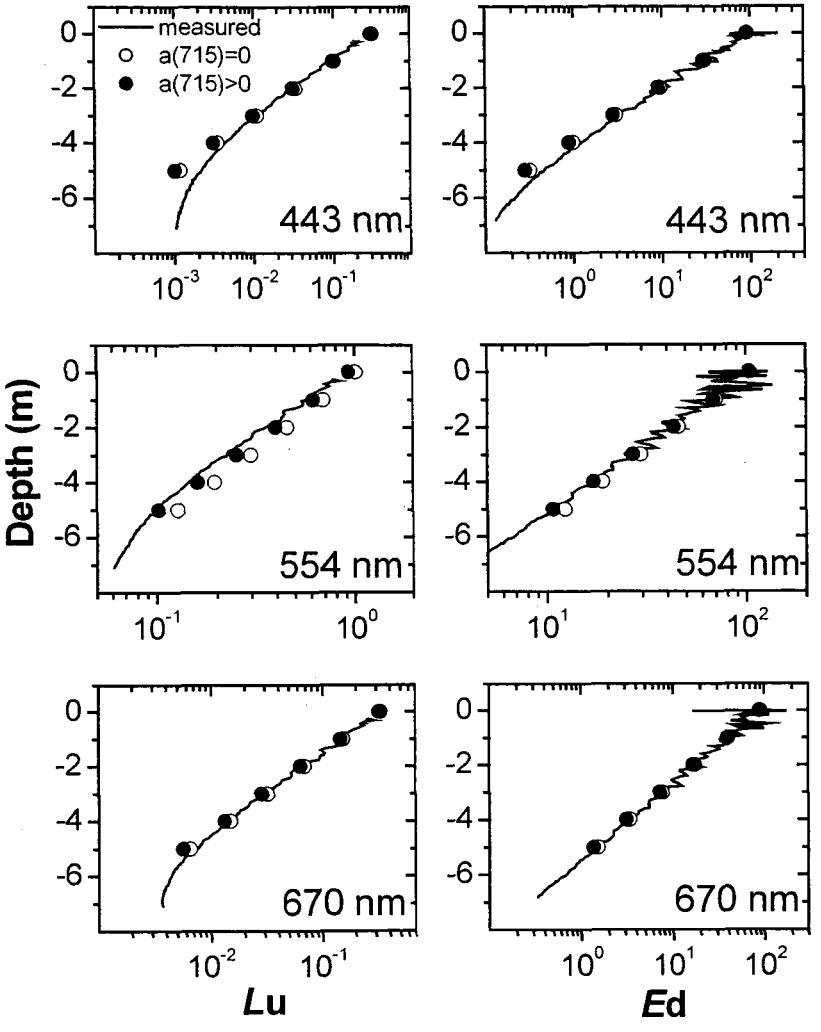

Figure 6, Tzortziou et al.,

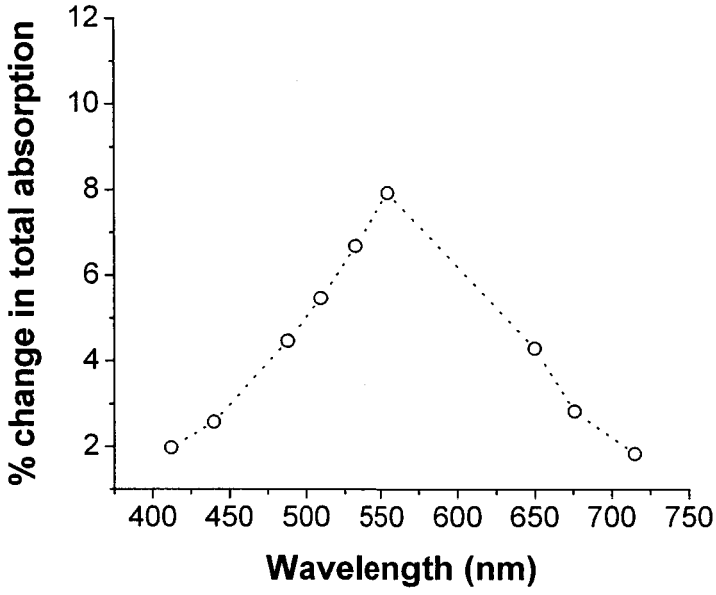

Figure 7, Tzortziou et al.,

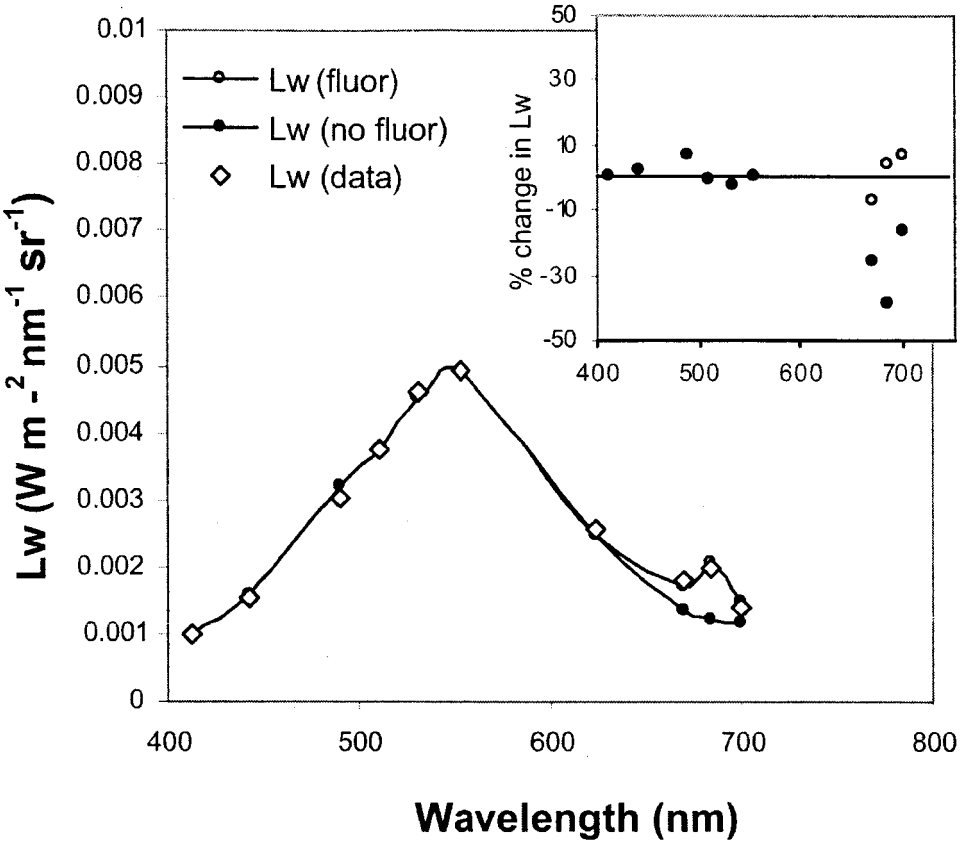

Figure 8, Tzortziou et al.,

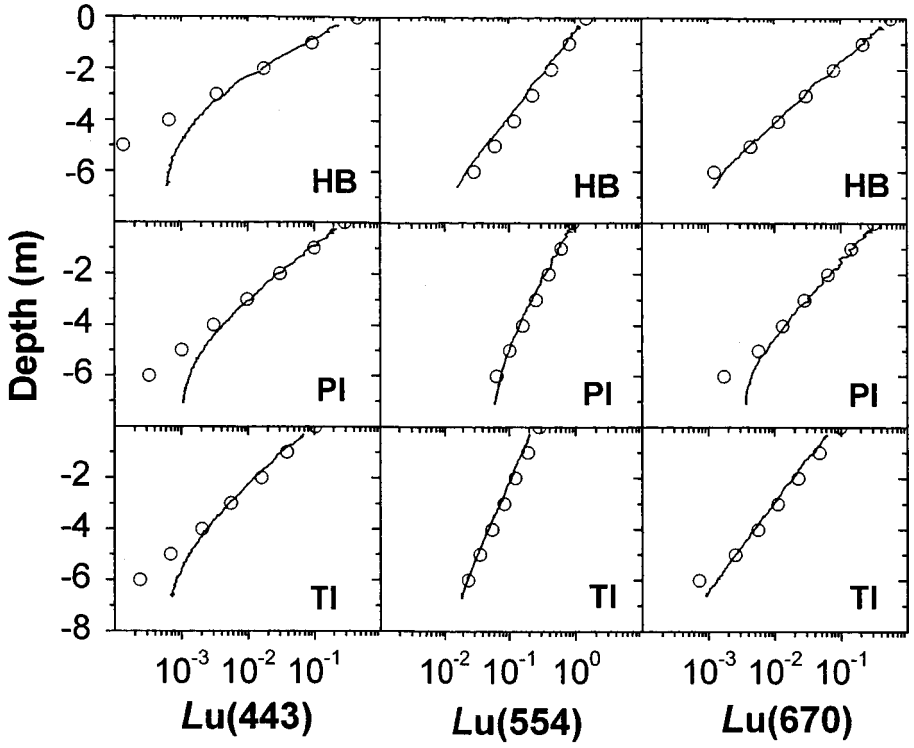

(a)

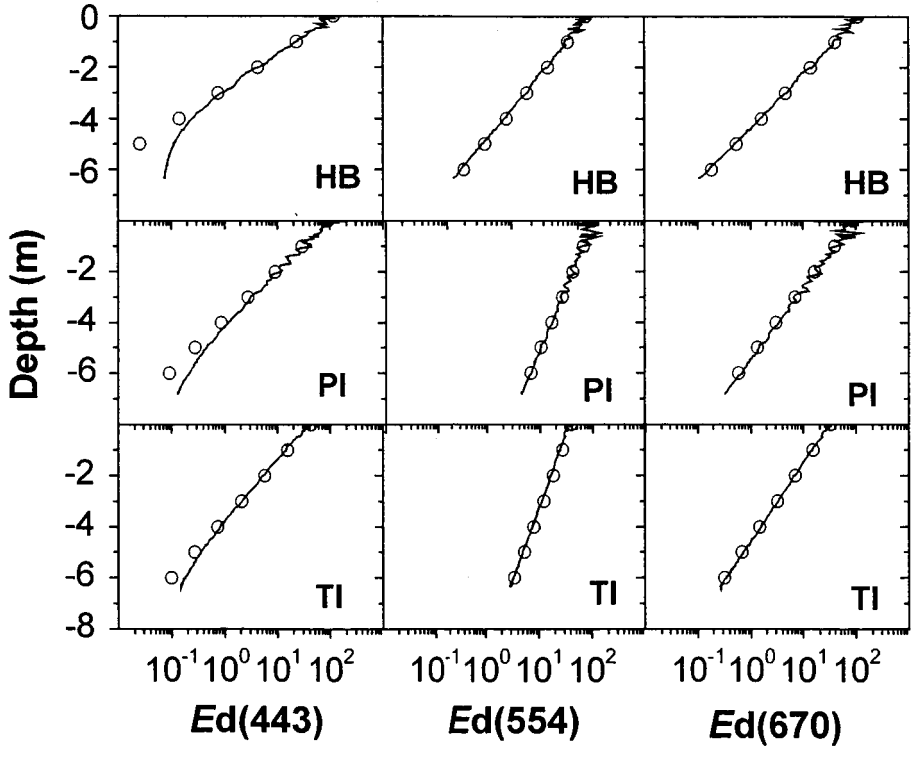

(b)

Figure 9, Tzortziou et al.,

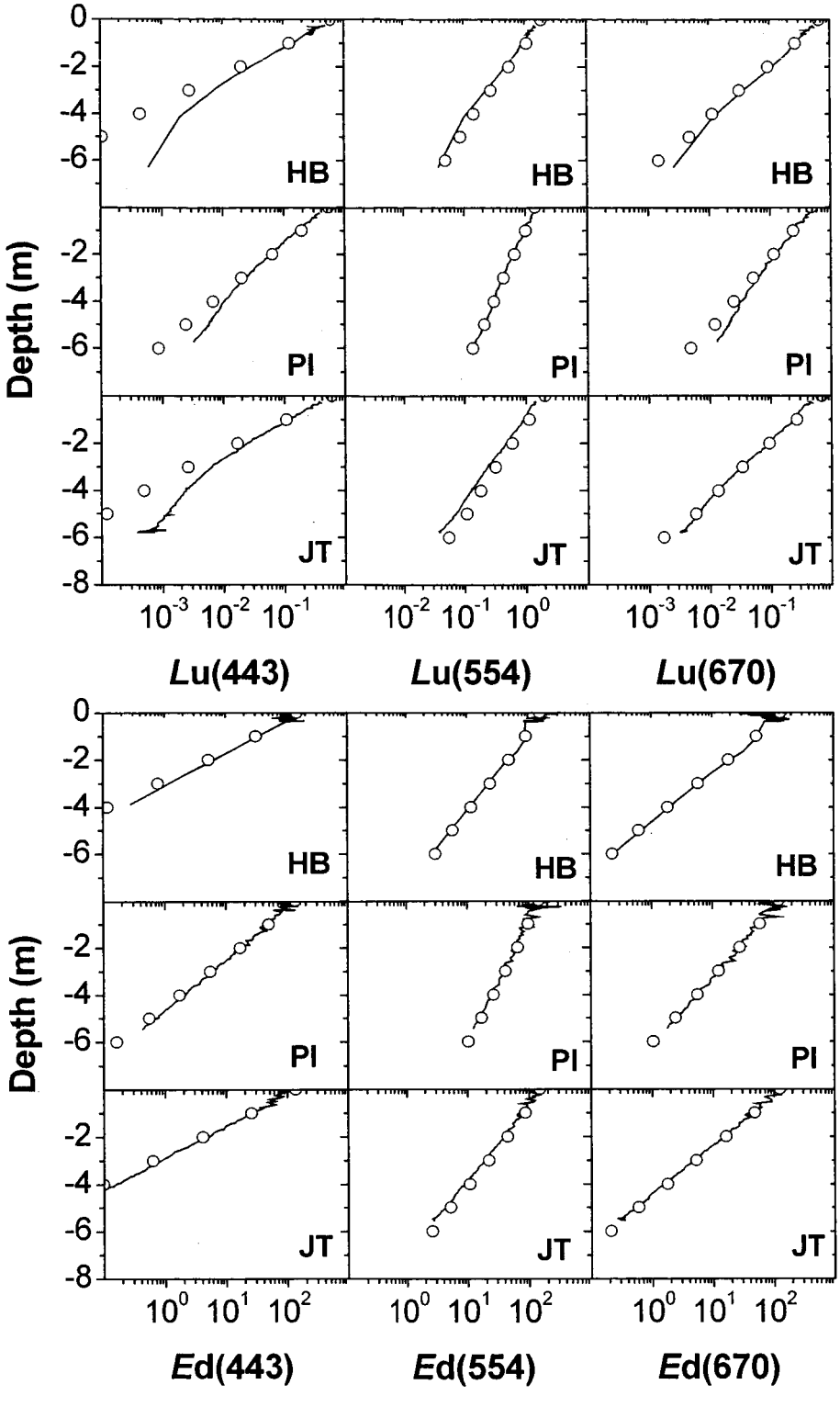

(a)

(b)

Figure 10, Tzortziou et al.,

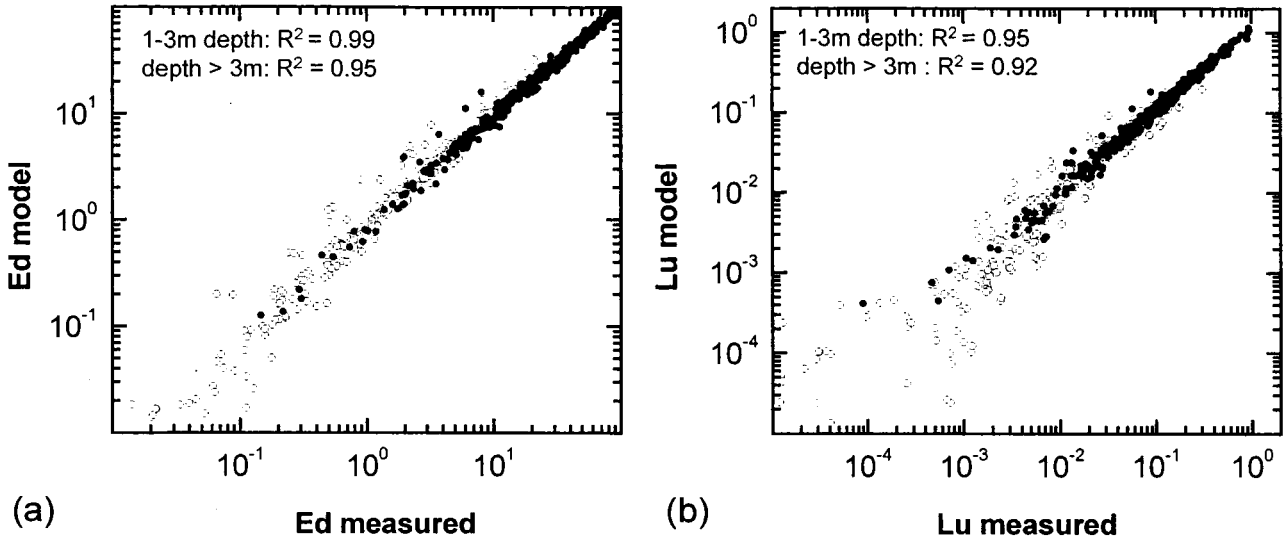

Figure 11, Tzortziou et al.,

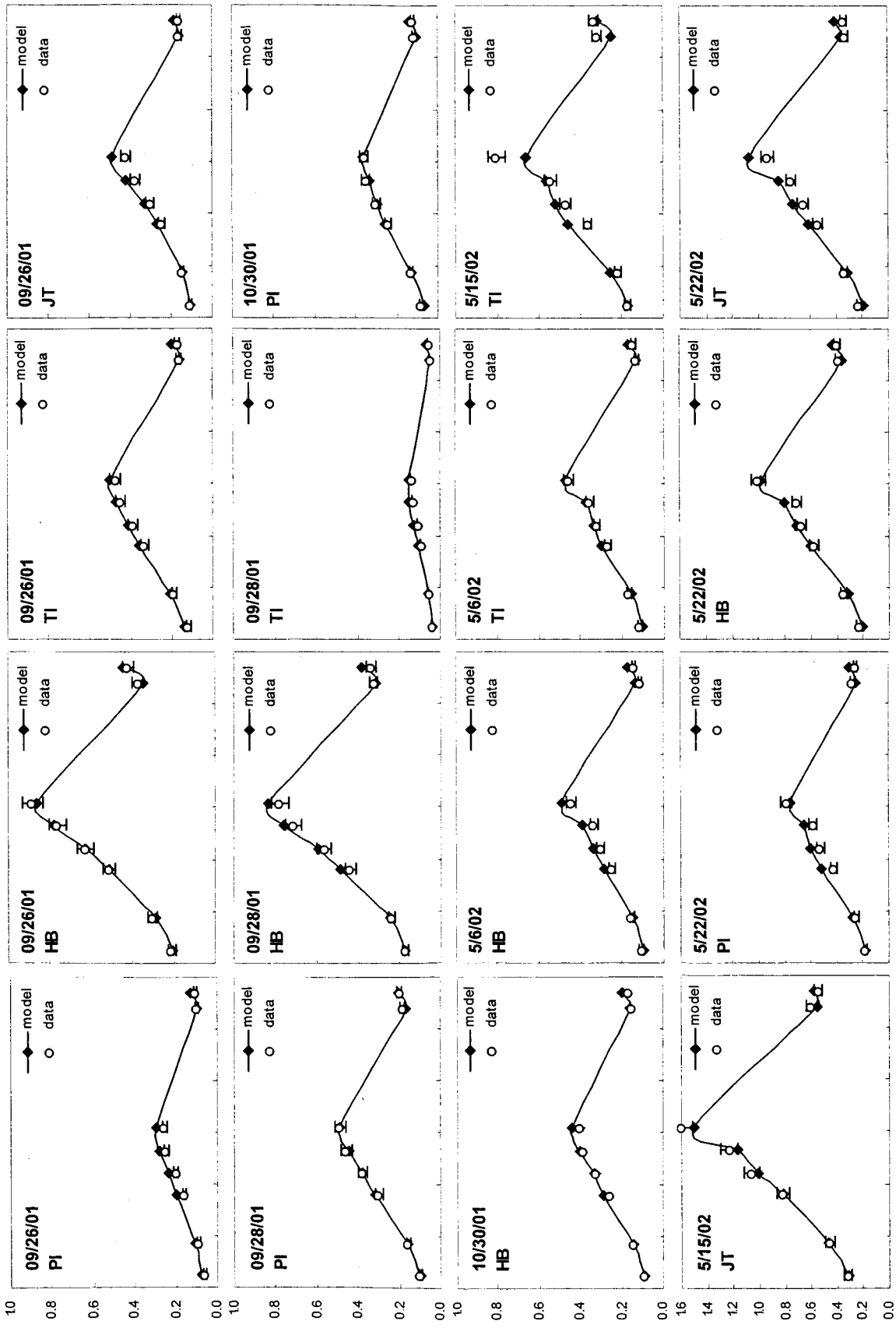
09/26/01 PI
09/26/01 HB
09/26/01 TI
09/26/01 JT
09/28/01 PI
09/28/01 HB
09/28/01 TI
10/30/01 PI
10/30/01 HB
5/6/02 HB
5/6/02 TI
5/15/02 TI
5/15/02 JT
5/22/02 PI
5/22/02 HB
5/22/02 JT
model
data
Wavelength (nm)
Lw (in μW nm-1 cm-2 sr-1)

(from previous page)

Figure 12, Tzortziou et al.,

Table 1: Dates of cruises in the Chesapeake Bay, and instrumentation for measurements of radiation fields. The AC9 and ECOVSF3 instruments were used in all cruises for measurements of water IOPs. Asterisks indicate cruises used for RT model simulations.

Date of cruise	**Instrument used for radiation fields**
2001, June 4	Satlantic OCI-200
2001, June 11	Satlantic OCI-200
2001, June 25	Satlantic OCI-200
2001, July 9	Satlantic OCI-200
2001, September 21	Satlantic SMSR
2001, September 26	Satlantic MicroPro *
2001, September 28	Satlantic MicroPro *
2001, October 4	Satlantic OCI-200
2001, October 30	Satlantic MicroPro *
2001, November 13	Satlantic OCI-200
2002, May 6	Satlantic MicroPro *
2002, May 15	Satlantic MicroPro *
2002, May 22	Satlantic MicroPro *
2002, June 6	Satlantic OCI-200
2002, June 18	Satlantic OCI-200
2002, June 28	-
2002, November 8	Satlantic MicroPro

Table 2: Measurements of IOPs and radiation fields in the Chesapeake Bay

Measured Quantity	Wavelength-range (in nm)	Instrument Used
Total absorption (minus absorption by pure water), $a_{t\text{-}w}$	412, 440, 488, 510, 532, 554, 650, 676, 715	AC-9
Total attenuation (minus attenuation by pure water), $c_{t\text{-}w}$	412, 440, 488, 510, 532, 554, 650, 676, 715	AC-9
Total backscattering, b_b	450, 530, 650	ECOVSF3
Chlorophyll-a concentration, [chl-a]		Spectrophotometric measurements
Phytoplankton absorption, a_{phyt}	290 – 750	CARY-IV spectrophotometer
Non-algal particulate absorption, a_{nap}	290 – 750	CARY-IV spectrophotometer
CDOM absorption, a_{CDOM}	290 – 750	CARY-IV spectrophotometer
In-water Upwelling radiance profiles, *L*u	400, 412, 443, 455, 490, 510, 532, 554, 564, 590, 625, 670, 684, 700	Satlantic, MicroPro
In-water Downwelling irradiance profiles, *E*d	400, 412, 443, 455, 490, 510, 532, 554, 564, 590, 625, 670, 684, 700	Satlantic, MicroPro
In-water Upwelling irradiance profiles, *E*u	412, 443, 490, 510, 554, 665, 684	Satlantic, OCI-200
In-water Downwelling irradiance profiles, *E*d	325, 340, 380, 412, 443, 490, 510, 532, 554, 620, 665, 684, 706	Satlantic, OCI-200
Above-water Surface Downwelling Irradiance, *E*s	400, 412, 443, 455, 490, 510, 532, 554, 564, 590, 625, 670, 684, 700	Satlantic OCR-507 Irradiance Sensors

Table 3: Range of values (min-max) of IOPs for those days for which Hydrolight simulations were performed. These span about 80-85% of observed values during all seventeen cruises in the Chesapeake Bay waters.

	$a_{t\text{-}w}(440)$ (m^{-1})	$a_{t\text{-}w}(676)$ (m^{-1})	$c_{t\text{-}w}(440)$ (m^{-1})	$c_{t\text{-}w}(676)$ (m^{-1})	b_b/b (530)	[chl-a] ($mg\ m^{-3}$)
min	0.6	0.12	2.5	1.6	0.006	4.8
max	1.44	0.44	8.5	6.3	0.020	23

Table 4: Improvement of agreement between measured and model-estimated Lw as information on the specific IOPs measured at station PI (28 September 2001) is successively incorporated into the RT model. The final agreement between data and model demonstrates the good optical closure obtained at this study site after applying the results from our detailed measurements to properly account in the RT modeling for the observed optical characteristics.

RT modeling	**Absolute % difference between model and data**
1. $a_{t\text{-}w}(715)=0$, fluorescence included, Petzold VSF	for Lw(554): 50%
2. FF VSF with $b_b/b=0.015$ (otherwise 1)	for Lw(554): 20%
3. FF VSF with $b_b/b(\lambda,z)$ (otherwise 1)	for Lw(554): 9%
4. $a_{t\text{-}w}(715)=a_{CARY}(715)$ (otherwise 3)	for Lw(554): 0.6% for Lw(685): 4%
5. chl-a fluorescence not included (otherwise 4)	for Lw(685): 40%

Table 5: (A) Percent differences in estimated *Lu* at 1 m depth (for wavelengths 443, 554, 670 nm) between in-situ measurements and model simulations, for measurements at stations representative of the clearest (28 September 2001) and most turbid (22 May 2002) waters we observed. Percent differences were estimated as: $\frac{Lu_{(model)} - Lu_{(data)}}{\frac{1}{2}(Lu_{(model)} + Lu_{(data)})} \cdot 100 \cdot$

(B) Similarly, for *Ed* at 1 m depth.

Table 5A

Lu	Wavelength (in nm)		
Station/Date	**443**	**554**	**670**
PI, 9/28/01	3.4	5.8	-8.8
HB, 9/28/01	17.2	18.8	3.5
TI, 9/28/01	12.9	19.2	22.1
PI, 5/22/02	17.4	7.4	0.6
HB, 5/22/02	-4.1	11.6	5.6
JT, 5/22/02	-15.5	16.4	6.7

Table 5B

Ed	Wavelength (in nm)		
Station/Date	**443**	**554**	**670**
PI, 9/28/01	-18.3	-0.9	-9.6
HB, 9/28/01	-1.6	7.9	4.3
TI, 9/28/01	7.1	12.4	5.1
PI, 5/22/02	3.5	6.4	5.5
HB, 5/22/02	8.9	0.4	0.8
JT, 5/22/02	-2.9	9	5.8

Table 6: Percent differences in estimated Lw values at various wavelengths (412-685 nm) using in-situ measurements and model simulations. Percent differences were estimated as:

$$\frac{Lw_{(model)} - Lw_{(data)}}{\frac{1}{2}(Lw_{(model)} + Lw_{(data)})} \cdot 100 \cdot$$

	Wavelengths (in nm)						
Station/Date	**412**	**443**	**490**	**532**	**554**	**670**	**685**
PI, 9/26/01	-21.7	-19.4	-22.3	-13.1	-14.3	-0.3	-15.8
HB, 9/26/01	-2.7	-5.5	-0.1	2.1	-2.8	-7.4	5
TI, 9/26/01	12.9	8.5	6.6	5.1	5.1	-0.6	15
JT, 9/26/01	1.8	-0.6	7.3	12	15.2	2.1	11.3
PI, 9/28/01	0.8	1.9	6.4	-2	0.6	-7.7	4.3
HB, 9/28/01	0.6	2.9	10.3	5.5	7	-3	11.7
TI, 9/28/01	-4.7	1.1	16.6	14	12.8	8	20.3
PI, 10/30/01	-19.7	-2.1	7.2	-4.6	1.2	-3.9	14.4
HB, 10/30/01	0.6	1.5	10.2	2.8	9.5	1.4	17
HB, 5/6/02	-10	-1.7	14.1	15.3	10	18.2	21.6
TI, 5/6/02	-14	-7.5	9.5	4.8	2.3	3.1	16.3
TI, 5/15/02	-1.9	15.9	22.7	3.8	-18.6	-22.4	-4.2
JT, 5/15/02	-2.8	1.9	-0.1	-5.1	-6.1	-7	5.9
PI, 5/22/02	-2.3	11.6	18.7	10.1	-2.7	-6.5	15.5
HB, 5/22/02	-11.5	-11	3.7	12.1	-1.8	-6.6	9.1
JT, 5/22/02	-13.6	-8.5	12.1	11.8	13.7	11.5	19.9
Average Absolute Percent Differences	**7.60**	**6.35**	**10.49**	**7.76**	**7.73**	**6.86**	**12.96**